Supplementary Information (SI) for Chemical Communications.
This journal is © The Royal Society of Chemistry 2024

SUPPORTING INFORMATION

Temperature-Dependent Li-Ion Transport in Lithium Lanthanum Titanates Electrolytes

Jiacheng Wang,[a] *Nianqiang Wu*[a] *and Peng Bai**[a]

[a] Department of Chemical Engineering, University of Massachusetts Amherst, Amherst, Massachusetts 01003-9303, USA

AUTHOR INFORMATION

Corresponding Author

* pengbai@umass.edu

I. Computational Details

The metadynamics simulations[1,2] were conducted with ab-initio molecular dynamics and non-spin-polarized, periodic density-functional theory (DFT) using the Vienna Ab initio Simulation Package (VASP),[3,4] version 6.1.2. The calculations used an experimentally determined LLTO unit cell with an elemental composition of $Li_6La_{10}Ti_{18}O_{54}$,[5] which belongs to the tetragonal lattice and has unit-cell parameters of $a = c = 11.636$ Å and $b = 7.905$ Å. Our test calculations for the pristine LLTO structure found little effect of spin polarization on relative energies, an observation that has been reported in DFT studies on similar systems.[6–8] The SCF cycles were converged to a criterion of 10^{-4} eV using a k-point grid of 1×2×1 and the Perdew-Burke-Ernzerhof (PBE) exchange-correlation functional.[9] Valence electrons were expanded using a plane-wave basis set with a kinetic energy cutoff of 400 eV while the core electrons were treated using the projector augmented wave (PAW) method,[10] which includes 1 (Li), 11 (La), 4 (Ti), and 6 (O) valence electrons. The time step was set to 1 fs, and the temperature was maintained using a Nosé-Hoover thermostat.[11]

Three relative coordinates were used as the collective variables: $\xi = \{\xi_a, \xi_b, \xi_c\}$ constructed as follows.

$$\xi_a = q_{\mathrm{Li},a} - \frac{1}{N}\sum_{i=1}^{N} q_{i,a} \tag{1}$$

$$\xi_b = q_{\mathrm{Li},b} - \frac{1}{N}\sum_{i=1}^{N} q_{i,b} \tag{2}$$

$$\xi_c = q_{\mathrm{Li},c} - \frac{1}{N}\sum_{i=1}^{N} q_{i,c} \tag{3}$$

where $N = 8$ is the number of reference atoms, which include four O atoms and four Ti atoms on the (100), (010), and (001) planes for ξ_a, ξ_b, and ξ_c, respectively. q_{Li} represent the Cartesian coordinates of a single Li^+ ion in the metadynamics simulations and q_i represent the Cartesian coordinates of the

i^{th} reference atom. Gaussian bias potentials with a height of h = 0.02 eV and a width of σ = 0.5 Å were added during the simulations at a frequency of t_G = 500 fs. To ensure thorough sampling, a wall of Gaussian restraining potentials with a width of σ = 0.5 Ang was applied at a distance of 1.9 Å outside the Ti_8 cage boundaries so that the Li^+ ion does not wander into neighboring Ti_8 cages. The simulation length is 50 ps for T = 100, 700, and 1000 K and 75 ps for T = 300 K.

The nudged-elastic band (NEB) calculations used a 1 × 2 × 1 supercell of the same LLTO unit-cell structure as described above, which resulted in a simulation box with $a = c$ = 11.636 Å, b = 15.810 Å, and an elemental composition of $Li_{12}La_{20}Ti_{36}O_{108}$. The original NEB method[12,13] followed by the climbing image NEB (CI-NEB)[14] was used with seven images to reach a force convergence threshold of 0.03 eV/Å. A 3 × 2 × 3 k-point grid and an SCF criterion of 10^{-6} eV were used in the NEB calculations, while all other computational details remained the same as above.

To examine the effect of DFT functionals, additional test calculations were conducted using PBE with Grimme-type D3 corrections and the Becke-Johnson damping[15] and the strongly constrained and appropriately normed (SCAN)[16] meta-GGA functional. Single-point calculations of the initial and transition states from the converged NEB calculations were performed for the pristine LLTO structure and the LLTO structure with a nitrogen dopant in the La-poor layer (ND@La-poor). Using PBE-D3-BJ, the forward hopping barriers are 0.27 and 0.18 eV for the pristine and ND@La-poor structures, respectively. These values are essentially identical as those from PBE (see Table S1). Using SCAN, the forward hopping barriers are 0.32 and 0.21 eV for the pristine and ND@La-poor structures, respectively, which are 0.03 – 0.04 eV too high. Since both barriers shift in the same direction, the difference between the two mechanisms is only 0.01 eV higher with SCAN than that with PBE. These comparisons suggest that relative energy differences of LLTO materials with a fixed stoichiometry are not overly sensitive to the choice of (local) DFT functionals and dispersive corrections.

II. Projection of 3D Free Energy Surfaces

The metadynamics simulations yielded 3D free energy surfaces (FES), $F(a,b,c)$, which were projected to give various 1D potentials of mean force depending on the temperature, presented in Figure 3.

At the two lower temperatures, T = 100 and 300 K, Li^+ ion hopping pathways are roughly quarter arcs (see Fig. S1a). The NEB method was used on the midplane in the (010) direction to determine the precise minimum-free-energy pathways, which were then parametrized using a set of equidistance points, $\tilde{q}_j$. $F(a,b,c)$ was projected onto the corresponding hopping pathways by reweighting using the following parameter:[17]

$$\xi_1 = \frac{1}{N-1}\frac{\sum_{i=1}^{N}(i-1)\exp\left[-\sum_{j=1}^{M}\left(q_j-\tilde{q}_j(i)\right)^2\right]}{\sum_{i=1}^{N}\exp\left[-\sum_{j=1}^{M}\left(q_j-\tilde{q}_j(i)\right)^2\right]} \tag{4}$$

$$F(\xi_1) = -k_B T \ln[H(\xi_1)] \tag{5}$$

where N = 100 is the number of predefined points along the discretized path and M = 3 is the dimension of the collective variables. Some care must be taken to ensure that the free energy projection is not biased by the geometry of the phase space. For example, if a quarter cuboid is used instead, the phase space has a smaller volume near the end of a path than at the middle. To address this issue, the region considered for the projection to a particular path only includes points within a fixed planar distance. The distance threshold is taken to be $1/4$ of the average length of the four paths, which is 0.53 Å and 0.56 Å at T = 100 K and 300 K, respectively. This procedure results in a curved-wall-shaped region (see Fig. S1b) that includes the important, low free-energy points of $F(a,b,c)$.

At the two higher temperatures, T = 700 and 1000 K, Li^+ ion hops along straight lines parallel to one of the lattice vectors. The corresponding potentials of mean force $F(\xi_2)$, for example when $\xi_2 = a$, was obtained by integrating $F(a,b,c)$ over the b and c axes:

$$F(\xi_2 = a) = -k_{\mathrm{B}}T\ln\left[\iint g(a,b,c)\,\mathrm{d}b\mathrm{d}c\right] \tag{6}$$

$$g(a,b,c) = \exp\left[-\frac{F(a,b,c)}{k_{\mathrm{B}}T}\right] \tag{7}$$

where k_{B} is the Boltzmann constant and T is the temperature. The integration was performed numerically using the trapezoidal rule:

$$F(\xi_2) = -k_{\mathrm{B}}T\ln\left[\Delta b\Delta c\sum_{i=1}^{N_b}\sum_{j=1}^{N_c}\frac{g(a,b_i,c_j) + g(a,b_{i+1},c_j) + g(a,b_i,c_{j+1}) + g(a,b_{i+1},c_{j+1})}{4}\right] \tag{8}$$

where N_b and N_c represent the number of grid points in the *b* and *c* directions, respectively.

III. Ionic Conductivity

The rate constant, *k*, for an elementary hopping event can be calculated based on transition-state theory:

$$k = \frac{k_{\mathrm{B}}T}{h}\exp\left(-\frac{\Delta G^{\ddagger}}{k_{\mathrm{B}}T}\right) \tag{9}$$

where k_{B} is the Boltzmann constant, T is the temperature, h is the Planck constant, and $\Delta G^{\ddagger}$ is the free energy barrier. The diffusion coefficient, *D*, can then be calculated as follows:

$$D = \frac{1}{2dt}\lim_{t\to\infty}\langle r^2\rangle = \frac{a^2 n}{2dt} = \frac{a^2 k}{2d} \tag{10}$$

where $d = 2$ is the dimensionality of the diffusion geometry, *n* is the number of hopping events over time *t*, and $a = 2.74$ Å is the hopping distance, which is the length of the vector from a face center to an adjacent face center. Finally, the ionic conductivity can be calculated using the Nernst-Einstein equation:[18]

$$\lambda = \frac{|z|F^2 D}{RT} N \tag{11}$$

where z = +1 is the formal charge of the conducting ions, F is the Faraday constant, R is the molar gas constant, and N = 9308 mol/m^3 is the number of charge carriers per unit volume. At T = 300 K, the hopping rate constant was calculated to be k = 1.28×10^{10} s^{-1}, giving a diffusion coefficient D = 2.40×10^{-6} cm^2 s^{-1}, which yields an ionic conductivity of 8.3×10^{-2} S cm^{-1}. Note that these calculations assumed that 1) all quarter arcs have the same free-energy barrier of 0.16 eV at T = 300 K, 2) the transmission coefficient can be ignored, and 3) Li^+ ion hopping in La-poor layers will not be interrupted by occupied La^{3+} sites; both (2) and (3) will lead to reduced conductivity.

IV. Additional Figures and Tables

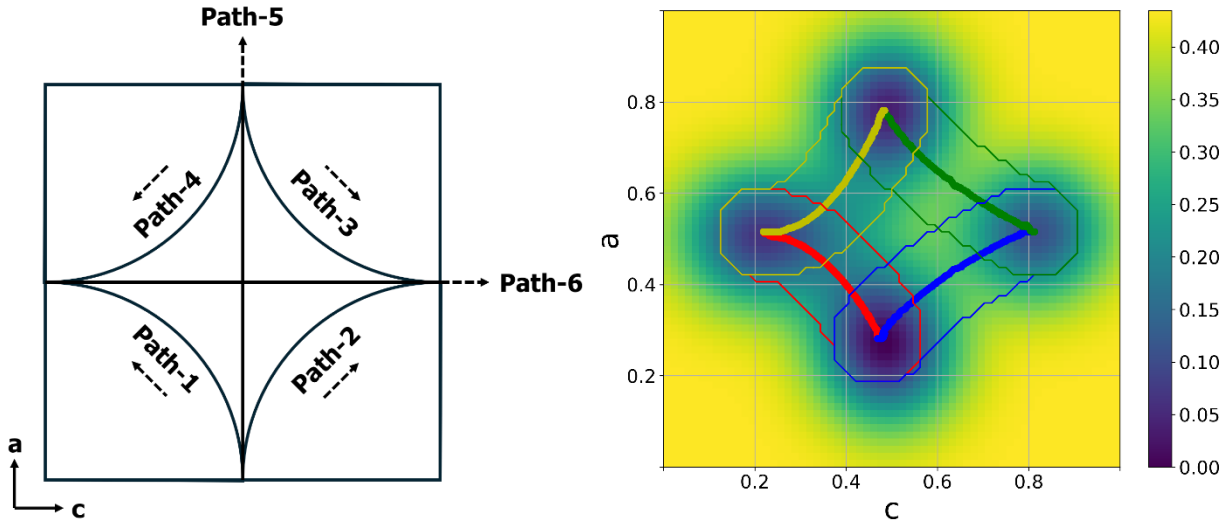

Figure S1. Left: Schematics of the six paths for 1D free-energy projection. Right: Illustration of the phase space regions included for projection to paths 1–4.

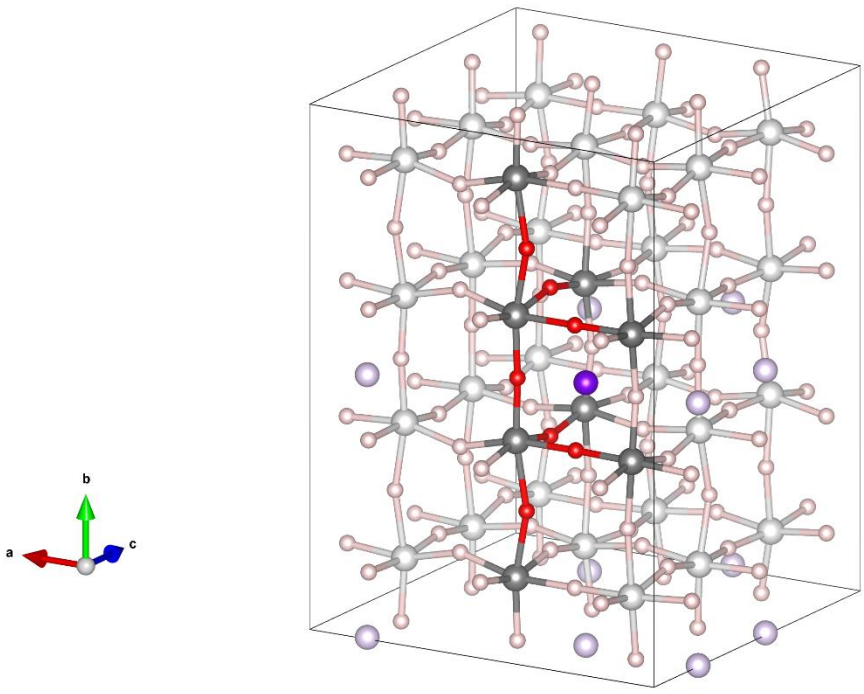

Figure S2. Initial state of the NEB calculations for Li^+ hopping in pristine LLTO materials. Li, Ti, and O atoms are shown in purple, silver, and red, respectively. For clarity, La atoms are hidden, and background atoms are shown in lighter hues.

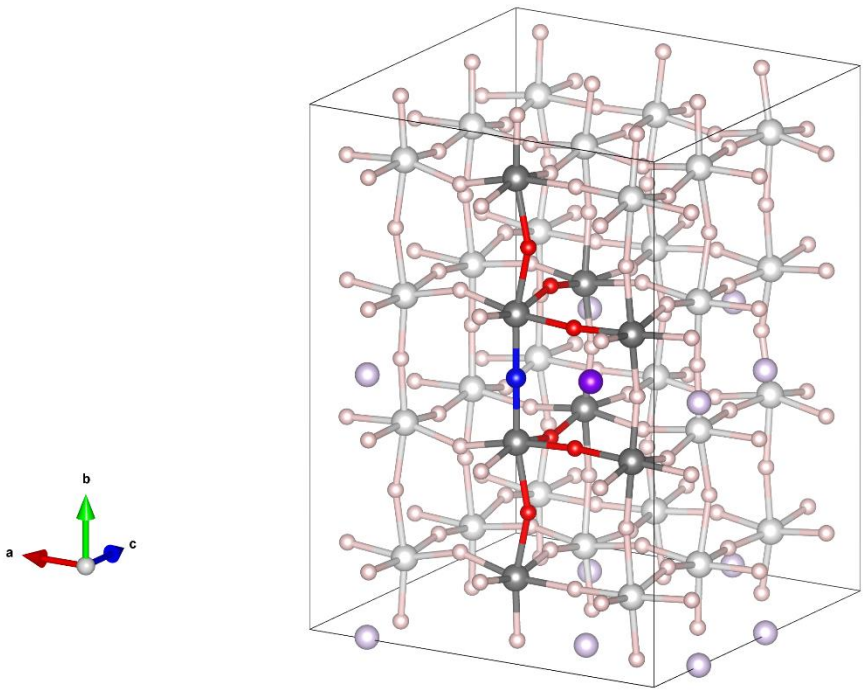

Figure S3. Initial state of the NEB calculations for Li^+ hopping in LLTO materials with a nitrogen dopant in the La-poor layer. Li, Ti, and O atoms are shown in purple, silver, and red, respectively. For clarity, La atoms are hidden, and background atoms are shown in lighter hues.

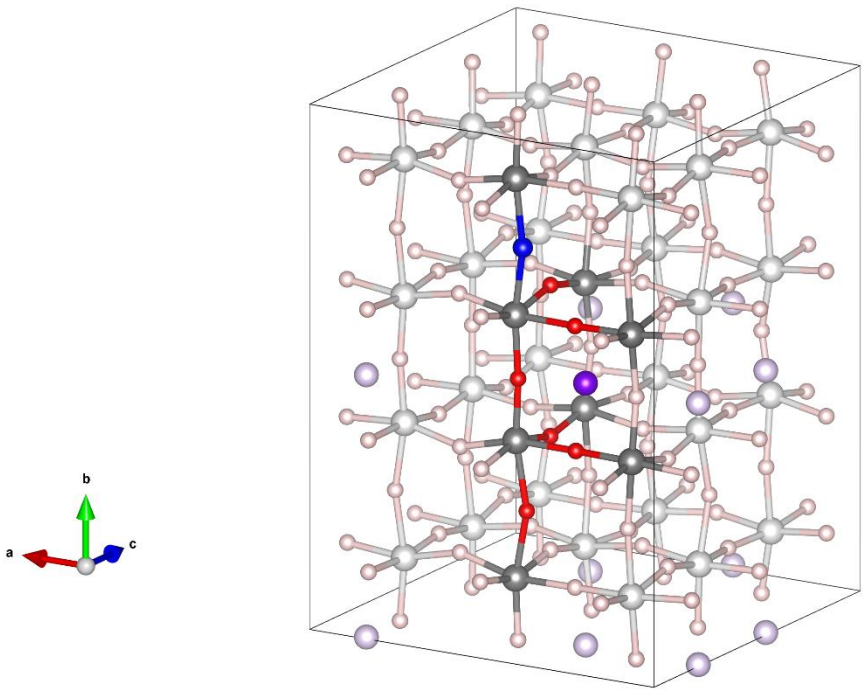

Figure S4. Initial state of the NEB calculations for Li^+ hopping in LLTO materials with a nitrogen dopant in the La-rich layer. Li, Ti, and O atoms are shown in purple, silver, and red, respectively. For clarity, La atoms are hidden, and background atoms are shown in lighter hues.

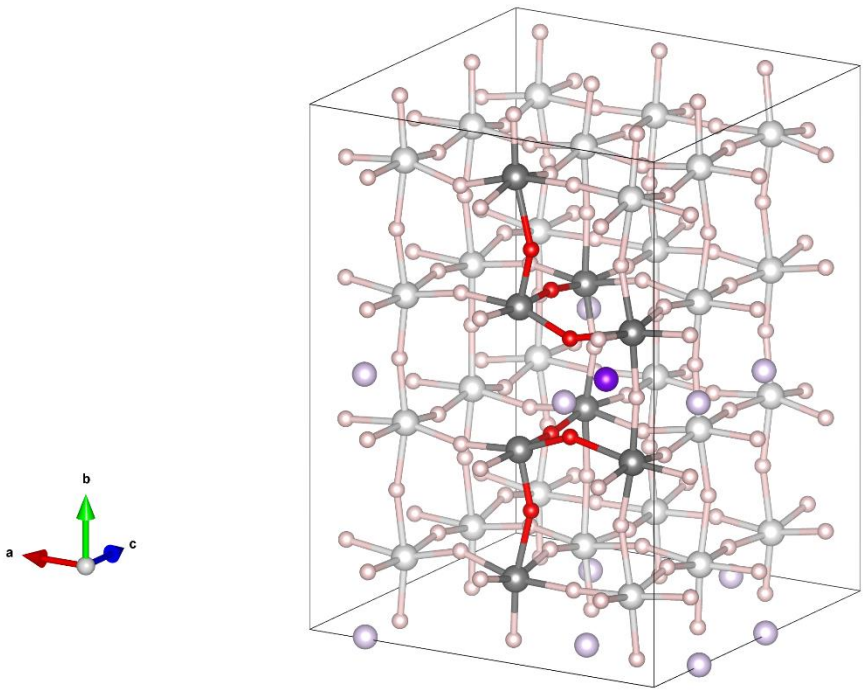

Figure S5. Initial state of the NEB calculations for Li^+ hopping in LLTO materials with an oxygen vacancy in the La-poor layer. Li, Ti, and O atoms are shown in purple, silver, and red, respectively. For clarity, La atoms are hidden, and background atoms are shown in lighter hues.

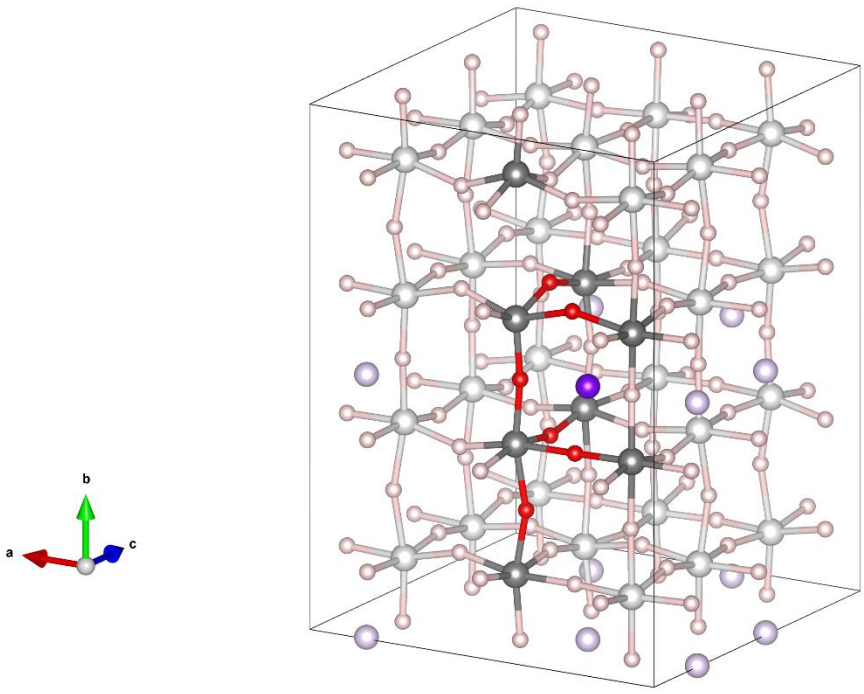

Figure S6. Initial state of the NEB calculations for Li^+ hopping in LLTO materials with an oxygen vacancy in the La-rich layer. Li, Ti, and O atoms are shown in purple, silver, and red, respectively. For clarity, La atoms are hidden, and background atoms are shown in lighter hues.

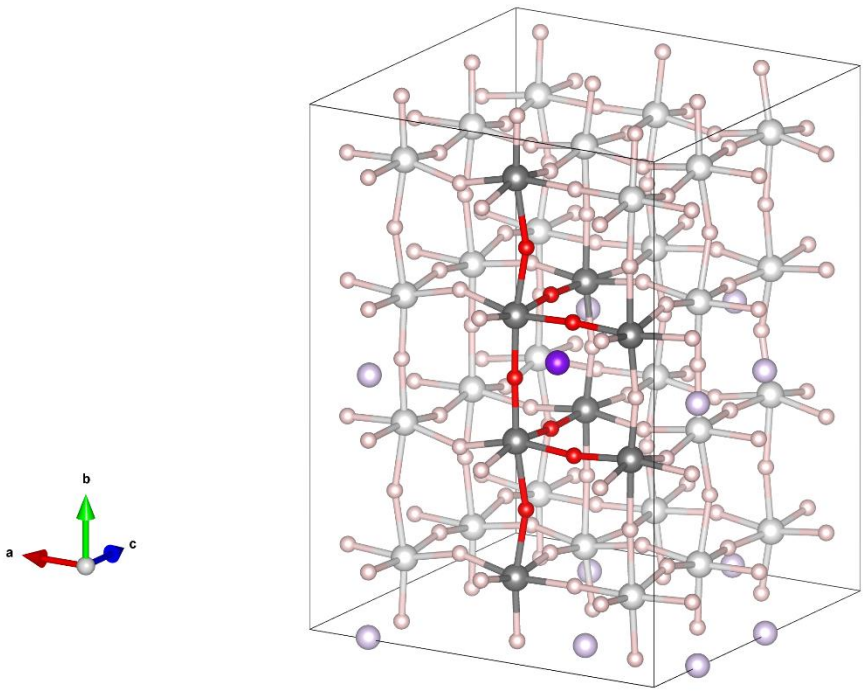

Figure S7. Final state of the NEB calculations for Li^+ hopping in pristine LLTO materials. Li, Ti, and O atoms are shown in purple, silver, and red, respectively. For clarity, La atoms are hidden, and background atoms are shown in lighter hues.

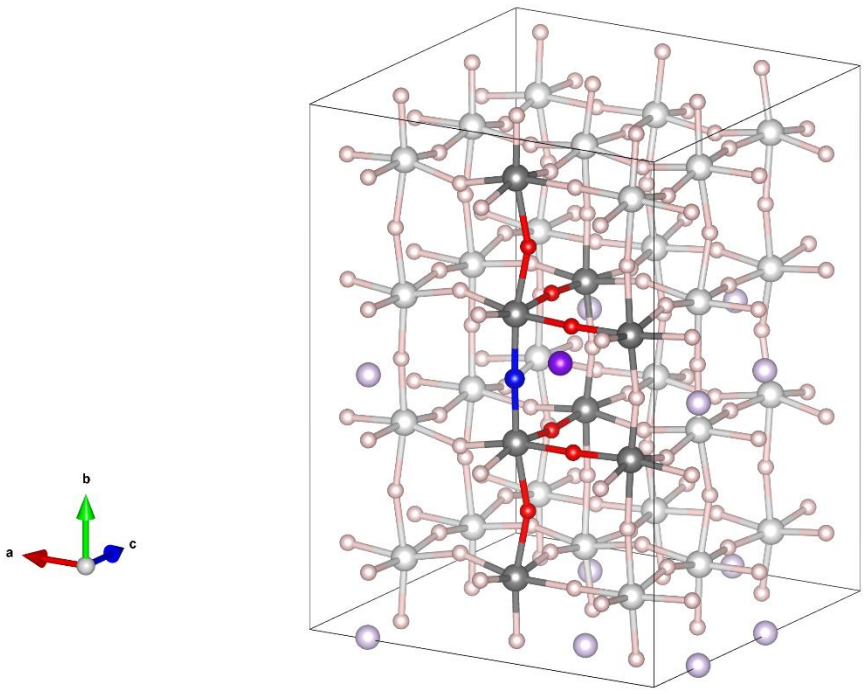

Figure S8. Final state of the NEB calculations for Li^+ hopping in LLTO materials with a nitrogen dopant in the La-poor layer. Li, Ti, and O atoms are shown in purple, silver, and red, respectively. For clarity, La atoms are hidden, and background atoms are shown in lighter hues.

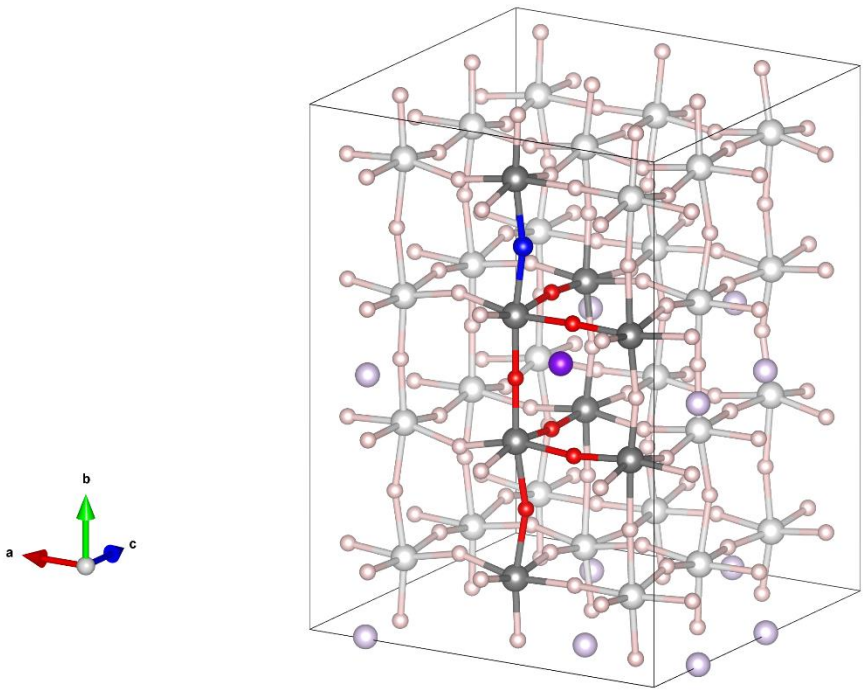

Figure S9. Final state of the NEB calculations for Li^+ hopping in LLTO materials with a nitrogen dopant in the La-rich layer. Li, Ti, and O atoms are shown in purple, silver, and red, respectively. For clarity, La atoms are hidden, and background atoms are shown in lighter hues.

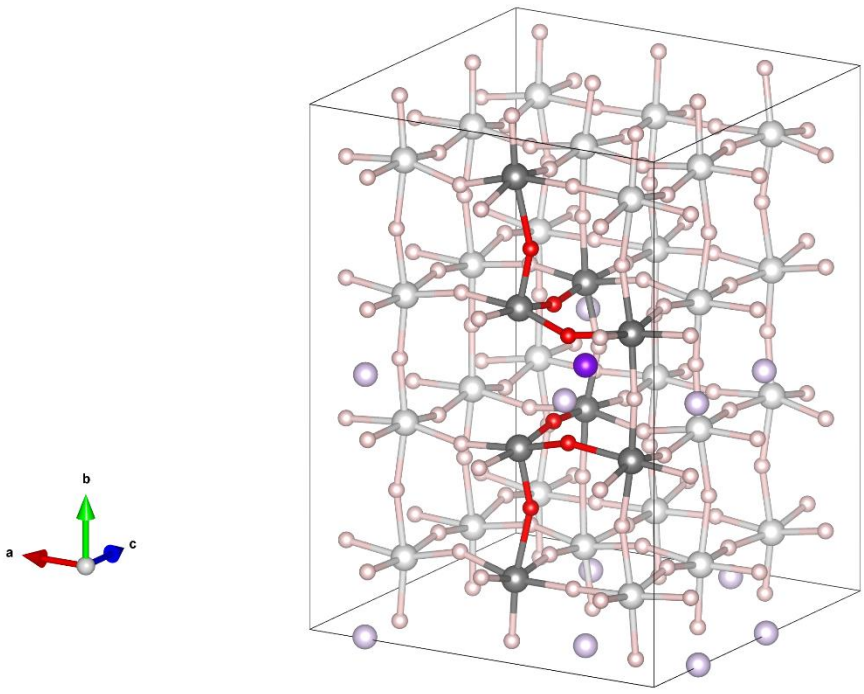

Figure S10. Final state of the NEB calculations for Li^+ hopping in LLTO materials with an oxygen vacancy in the La-poor layer. Li, Ti, and O atoms are shown in purple, silver, and red, respectively. For clarity, La atoms are hidden, and background atoms are shown in lighter hues.

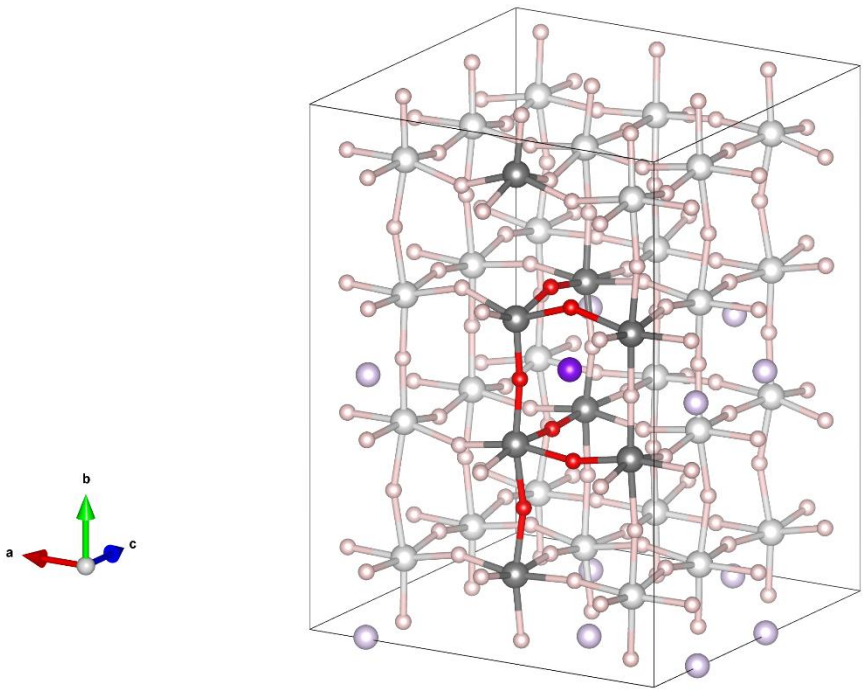

Figure S11. Final state of the NEB calculations for Li^+ hopping in LLTO materials with an oxygen vacancy in the La-rich layer. Li, Ti, and O atoms are shown in purple, silver, and red, respectively. For clarity, La atoms are hidden, and background atoms are shown in lighter hues.

Table S1. Energies (in eV) of initial, transition, and final states for Li^+ hopping in different LLTO materials as shown in Fig. 4. Bold numbers indicate the more stable state (initial or final) or the higher barrier (forward or reverse).

	pristine	ND@La-poor	ND@La-rich	OV@La-poor	OV@La-rich
Initial State	**0**	1.81	**1.71**	**9.27**	8.10
Transition State	0.28	1.99	2.00	9.44	8.21
Final State	0.05	**1.79**	1.83	9.28	**8.06**
Forward Barrier	**0.28**	0.18	**0.29**	**0.17**	0.12
Reverse Barrier	0.23	**0.19**	0.17	0.16	**0.15**

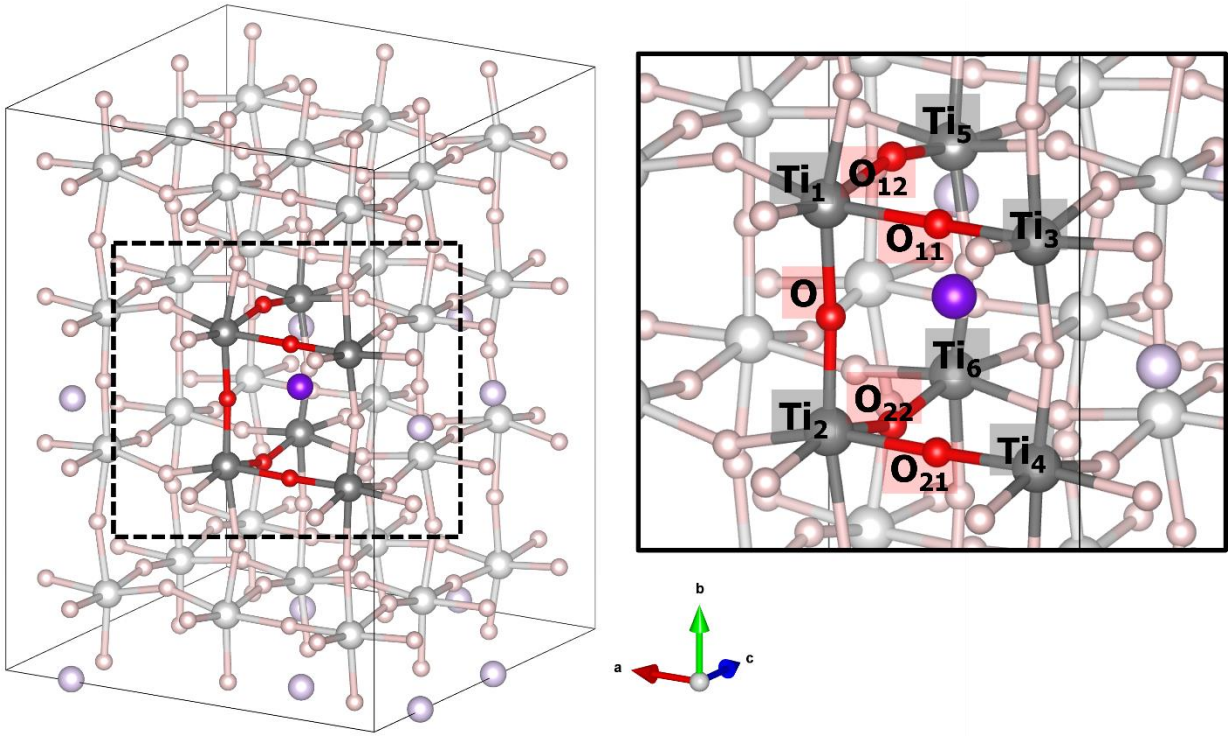

Table S2. Selected geometric parameters of initial states (IS), transition states (TS), and final states (FS) for Li^+ hopping in different LLTO materials as shown in Fig. 4.

structure	state	Ti_1-O/N-Ti_2	Ti_1-O_{11}-Ti_3	Ti_2-O_{21}-Ti_4	Ti_1-O_{12}-Ti_5	Ti_2-O_{22}-Ti_6
pristine	IS	176.7	177.5	176.1	160.1	158.8
	TS	171.1	171.2	174.8	163.1	158.1
	FS	175.2	172.5	170.5	174.3	173.5
ND@La-poor	IS	179.4	173.0	174.2	158.6	157.4
	TS	175.8	171.7	171.5	159.5	158.0
	FS	177.6	173.0	176.9	172.9	172.0
ND@La-rich	IS	175.4	177.0	176.2	156.5	158.0
	TS	169.5	173.7	174.0	157.6	159.1
	FS	175.0	173.4	170.7	170.2	173.0
OV@La-poor	IS	/	146.0	146.0	170.8	170.6
	TS	/	147.7	147.6	176.7	177.4
	FS	/	151.3	151.2	164.5	164.3
OV@La-rich	IS	171.7	155.4	176.8	146.9	162.0
	TS	167.8	148.1	172.1	146.7	167.3
	FS	172.8	147.8	164.0	155.8	175.3

References

1 A. Laio and M. Parrinello, *Proc. Natl. Acad. Sci. U.S.A.*, 2002, **99**, 12562–12566.

2 M. Iannuzzi, A. Laio and M. Parrinello, *Phys. Rev. Lett.*, 2003, **90**, 238302.

3 G. Kresse and J. Furthmüller, *Phys. Rev. B*, 1996, **54**, 11169–11186.

4 G. Kresse and J. Furthmüller, *Comp. Mater. Sci.*, 1996, **6**, 15–50.

5 H. Yang, K. Tay, Y. Xu, B. Rajbanshi, S. Kasani, J. Bright, J. Boryczka, C. Wang, P. Bai and N. Wu, *J. Electrochem. Soc.*, 2021, **168**, 110507.

6 J. Bhattacharya and A. Van Der Ven, *Phys. Rev. B*, 2010, **81**, 104304.

7 S. Ganapathy, A. Vasileiadis, J. R. Heringa and M. Wagemaker, *Adv. Energy Mater.*, 2017, **7**, 1601781.

8 T. Lee, J. Qi, C. A. Gadre, H. Huyan, S.-T. Ko, Y. Zuo, C. Du, J. Li, T. Aoki, R. Wu, J. Luo, S. P. Ong and X. Pan, *Nat. Commun.*, 2023, **14**, 1940.

9 J. P. Perdew, K. Burke and M. Ernzerhof, *Phys. Rev. Lett.*, 1996, **77**, 3865–3868.

10 G. Kresse and D. Joubert, *Phys. Rev. B*, 1999, **59**, 1758–1775.

11 S. Nosé, *Prog. Theor. Phys. Suppl.*, 1991, **103**, 1–46.

12 H. Jónsson, G. Mills and K. W. Jacobsen, in *Classical and Quantum Dynamics in Condensed Phase Simulations*, WORLD SCIENTIFIC, LERICI, Villa Marigola, 1998, pp. 385–404.

13 G. Henkelman and H. Jónsson, *J. Chem. Phys.*, 2000, **113**, 9978–9985.

14 G. Henkelman, B. P. Uberuaga and H. Jónsson, *J. Chem. Phys.*, 2000, **113**, 9901–9904.

15 S. Grimme, S. Ehrlich and L. Goerigk, *J Comput Chem*, 2011, **32**, 1456–1465.

16 J. Sun, A. Ruzsinszky and J. P. Perdew, *Phys. Rev. Lett.*, 2015, **115**, 036402.

17 D. Branduardi, F. L. Gervasio and M. Parrinello, *J. Comput. Phys.*, 2007, **126**, 054103.

18 J. Newman and N. P. Balsara, *Electrochemical systems*, John Wiley & Sons, 2021.